Malaysian NANO-An International Journal

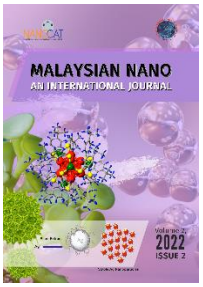

Research article

Received November 12, 2022
Revised November 19. 2022
Accepted December 8, 2022

DOI:
https://doi.org/10.22452/mnij.vol2no2.3

Corresponding authors:
jeyanthinath.chem@mkuniversity.org

Solvothermal synthesis and characterization of Iron oxide nanoparticles

R. Venkatesan[a], J. Mayandi[a*], S. Sagadevan[b*], V. Venkatachalapathy[c]

[a] *Department of Material Science, School of Chemistry, Madurai Kamaraj University, Tamilnadu, Madurai-625 021, India*
[b] *Nanotechnology and Catalysis Research Centre, Universiti Malaya, Kuala Lumpur, Malaysia –50603*
[c]*Department of Physics/Centre for Materials Science and Nanotechnology, University of Oslo, P.O, Box 1048 Blindern, NO-0316 Oslo, Norway*
[d]*Department of Materials Science, National Research Nuclear University "MEPhI", 31 Kashirskoesh, Moscow, Russian Federation*

Abstract

In the present study, we investigated the crystallinity, surface morphology, and optical properties of iron oxide (Fe_3O_4) nanoparticles (NPs) formed by solvothermal synthesis. From powder XRD analysis, the Fe_3O_4 NPs were found to be an inverse spinel structure and highly crystalline nature. The surface morphology and particle size distribution were analyzed using a scanning electron microscope (SEM). The elemental compositions were confirmed using energy-dispersive X-ray spectroscopy (EDX). The optical characteristics of the Fe_3O_4 NPs were analyzed by UV-Vis spectroscopy. Overall, from the analysis, Fe_3O_4 NPs with tailored optical and structural properties can be easily formed by the solvothermal route to find potential applications in industries and the medical field.

Keywords: Iron oxide, Solvothermal synthesis, Surface morphological and Optical properties

1. Introduction

Nanotechnology has received considerable attention as one of the most significant recent developments in the field of science and technology. One of the key components in creating and developing nanomaterials is the use of nanoparticles [1]. Thus, nanoparticles have drawn the attention of many researchers worldwide because of their unique properties such as shape, size, and distribution, which may be used in a variety of applications [2]. Iron oxide nanoparticles play a vital role in many fields of chemical, physical, and material science [3,4]. Iron oxides occur in a variety of forms, but magnetite (Fe_3O_4), maghemite (γ-Fe_2O_3), and hematite (α- Fe_2O_3) are particularly important in terms of technology [5-7]. Owing to their distinctive magnetic properties and favorable biocompatibility for potential applications in magnetic resonance imaging, drug delivery, and bio-separation, magnetite (Fe_3O_4) nanocrystals have received considerable attention [8-10]. Additionally, Fe_3O_4 has been proven to be an excellent nanostructured lithium-ion battery storage material. [11]. The identification of magnetic interactions in assembly systems is essential, especially for probing the magnetization of individual nanocrystals and determining the fringing field in the area [12].

There have been several synthesis routes for the formation of nanosized Fe_3O_4 with varying bandgap energies, and this property is strongly influenced by the manufacturing method, reaction temperature, use of surfactants as stabilizers, and extent of doping. Several techniques have been developed for the synthesis of Fe_3O_4 NPs in various phases, including the hydrothermal process [13], co-precipitation method [14], sol–gel route [15], microwave synthesis [16], microemulsion method [17], and ultrasound irradiation [18]. The resulting Fe_3O_4 exhibited various morphologies such as particles [19], belts [20], rings [21], and hollow spheres [22]. Therefore, in the present investigation, we employed solvothermal synthesis for the formation of Fe_3O_4 NPs and characterized their crystallinity and crystal nature, morphology, particle size distribution and optical properties.

2. Experimental Section

2.1. Materials

Iron chloride (ACS grade) and Ethylene glycol (GR grade) from MERCK India, Tri-sodium citrate-Dihydrate, and Sodium acetate (AR grade) are from SRL chemicals India. All the chemicals and solvents used during the synthesis were used as received without any further purification.

2.2. Synthesis of Fe_3O_4 NPs

To form Fe_3O_4 NPs, 50 ml of ethylene glycol and 2 g of $FeCl_3$ were added, and the solutions were mixed under constant magnetic stirring. After stirring for 5 min, 4 g of sodium acetate was added to

the mixture under vigorous magnetic stirring. After stirring for 5 min, 0.4 gm of trisodium citrate was added to the mixture. After another 30 min of stirring, the mixture was transferred to a stainless-steel autoclave and heated for 12 h at 200 °C and 250 °C and 4 h at 300 °C. The pressure at 200 °C was very minimum and at 250 °C it was about 410 pSi and for 300°C as high as 1350pSi so for the 300 °C the reaction was stopped at 4hr itself. The autoclave was then cooled to room temperature, and the product was magnetically separated, washed several times in distilled water, and dried at 60 °C for 5–6 h under ambient conditions.

2.3. Instrumental analysis

The crystal structure of the resulting powder samples was analyzed by x-ray diffraction (XRD, Rigaku, Cu Kα radiation, λ=1.5408 Å). The UV-Vis spectrometer (JASCO V-650 UV-VIS spectrophotometer) was employed to measure the absorbance. Scanning electron microscope (SEM, VEGA TESCAN 3 model) connected to an energy-dispersive X-ray (EDAX) detector and were used to analyze the morphology and elemental composition of the samples

3. Results and discussion

In this study, Fe_3O_4 NPs formed by solvothermal synthesis at different temperatures were analyzed for their crystallinity, crystal size, and phase purity using powder XRD analysis, where the diffraction patterns in the 2θ range of 10-80° are provided in Figure 1. Diffraction angles and peaks were observed at different reaction temperatures. At 200 °C, the Fe_3O_4 NPs exhibited reflection patterns along the crystal planes of (200), (311), (400), (422), (511), and (440), which can be attributed to the inverse spinel structure and confirmed that the resultant particles were pure Fe_3O_4 NPs. As shown in Fig. 1, the diffraction peaks of the Fe_3O_4 NPs reference can be assigned to the standard inverse spinel structure of Fe_3O_4 NPs (JCPDS 65-3107) with a=8.364 [23] and no diffraction peaks of other impurity were found. There is an additional peak around 37° in the XRD pattern at reaction temperatures of 250 °C and 300 °C which can be attributed to the (222) plane appearing due to pressure variations. The average sizes of the synthesized Fe_3O_4 NPs were estimated using Scherrer's equation

$$D = \frac{0.9\lambda}{\beta cos\theta} \quad (1)$$

where D is the average particle size (nm), λ is the incident X-ray wavelength (1.54Å), β is the full width at half maximum (FWHM) of reflected X-ray (radians) and θ is the position diffraction angle. The average crystalline sizes as calculated using the above equation are 10.88 nm, 16.43 nm, and 24.69 nm for reaction temperatures of 200, 250, and 300 °C, respectively, as calculated using the

above equation. As the reaction temperature increased, the average crystallite size also increased. This also indicates that the iron-oxide nanoparticles are crystalline solids of the magnetite phase.

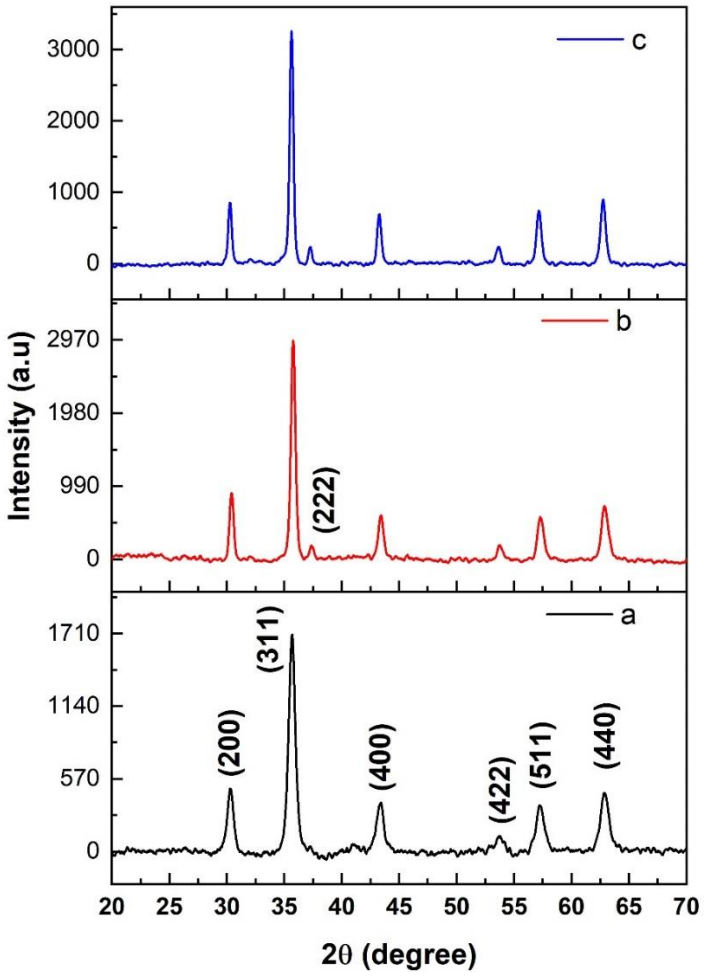

Figure 1: Powder XRD pattern of Fe_3O_4 NPs prepared at different temperatures a) 200 ^oC b) 250 ^oC c) 300 ^oC.

The particle size and morphology of Fe_3O_4 NPs at different temperatures and reaction times were examined using SEM. Figure 2 (a-c) shows the SEM images of as-prepared Fe_3O_4 NPs at different temperatures, where there is an aggregation or overlapping of smaller-sized Fe_3O_4 particles to generate larger particles. The synthesized magnetite nanoparticles were spherical [24].

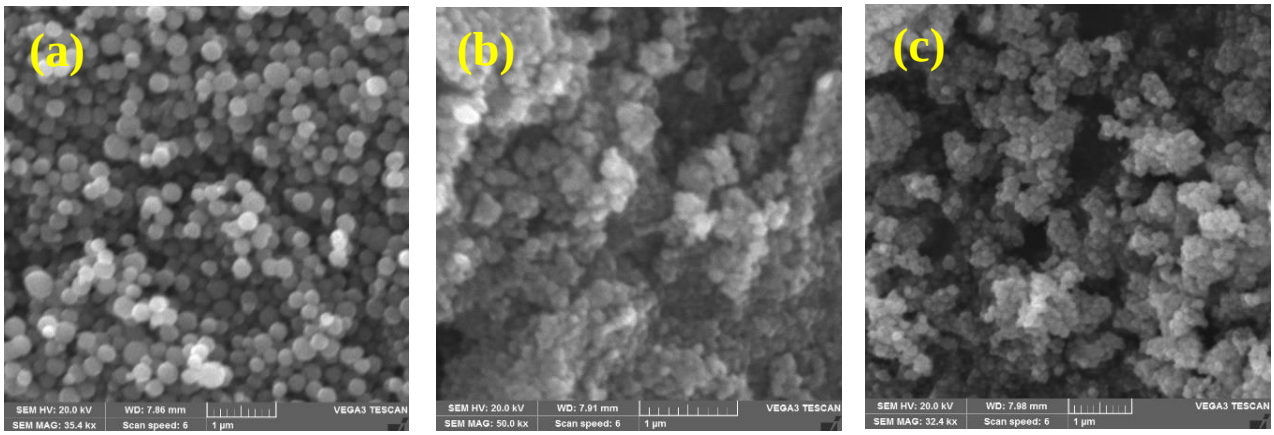

Figure 2: SEM image of synthesized Fe_3O_4 NPs a) 200 ^oC, b) 250 ^oC, c) 300 ^oC.

The average particle size distribution was calculated using ImageJ software, and the histogram is shown in Figure 3 (a-c). Figure 3 (a) indicates that the particles are spherical in shape and shows that the particle size ranged from 100 to 448 nm and the average particle size was 247 nm. Figure 3 (b). shows that the particle size ranged from 60 to 190 nm, and the average particle size was 114 nm. Figure 3 (c). shows the particle size ranges from 50 nm to 150 nm, and the average particle size is 104 nm. From this, we infer that the particle size decreased when the pressure increased during the experiment.

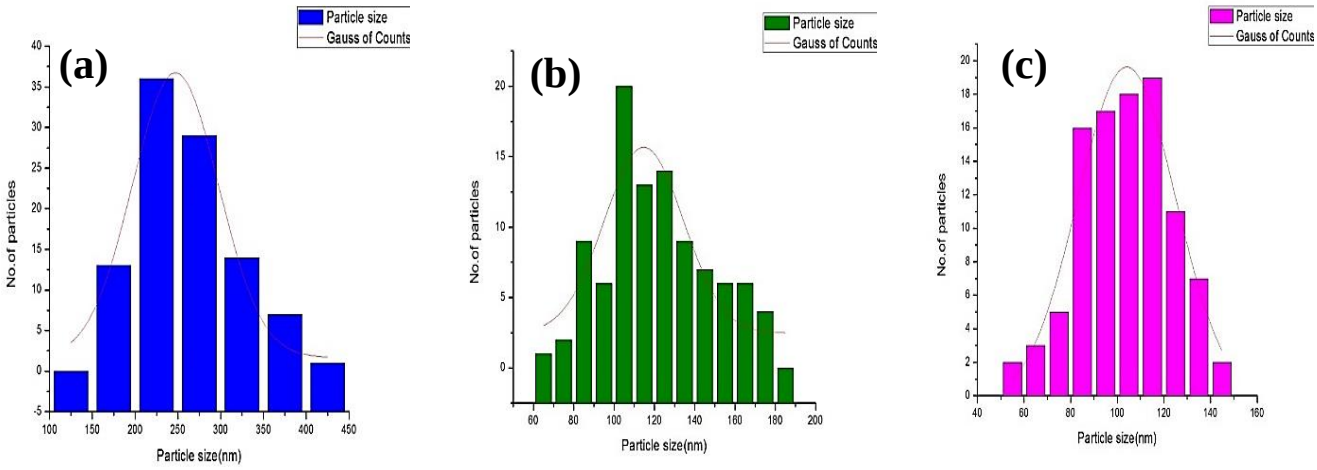

Figure 3 Particle size distribution of Fe_3O_4 NPs a) 200 ^oC, b) 250 ^oC, c) 300 ^oC calculated from SEM image.

Further, the EDX spectra in Figure 4 (a-c) confirm the formation of Fe_3O_4 NPs at different temperatures along with the atomic and weight percentages of the elements. The EDX spectra confirmed the presence of Fe and O in the powdered sample, thereby supporting high purity without any impurities.

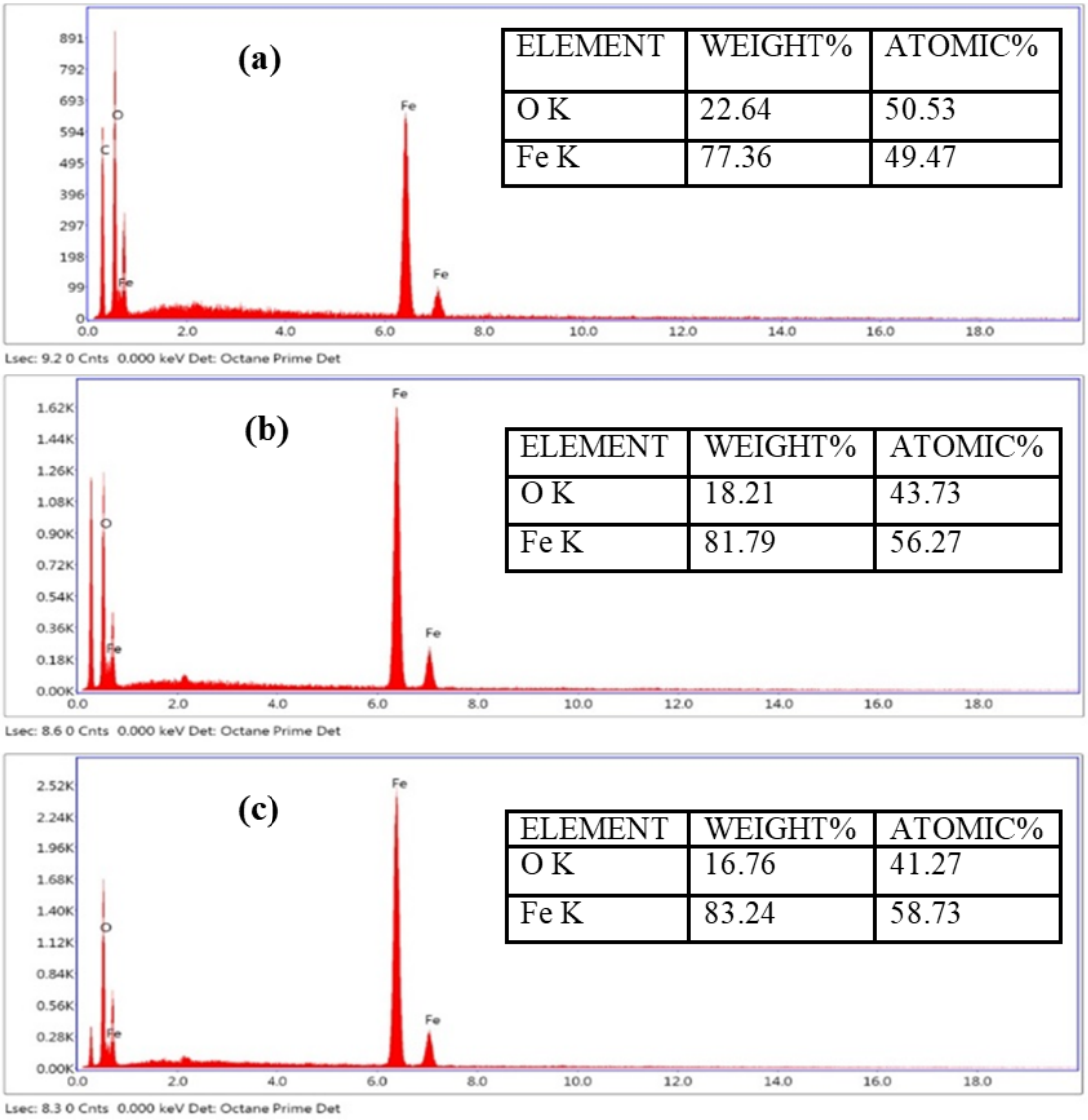

Figure 4: EDX spectra of Fe_3O_4 NPs a) 200 ^oC, b) 250 ^oC, c) 300 ^oC

To investigate the optical absorption of the magnetite nanoparticles, UV-VIS absorption spectra were measured. Figure 5 shows the absorption spectra of the magnetite nanoparticles at various reaction temperatures. As shown in Figure 5, for various temperatures, an absorption coefficient was recorded in the visible region in the wavelength range of 420–580 nm. The absorption edge of Fe_3O_4 exhibited a red shift when the reaction was performed at 200 °C. The absorption edge exhibited a blue shift at 250 and 300 °C [25].

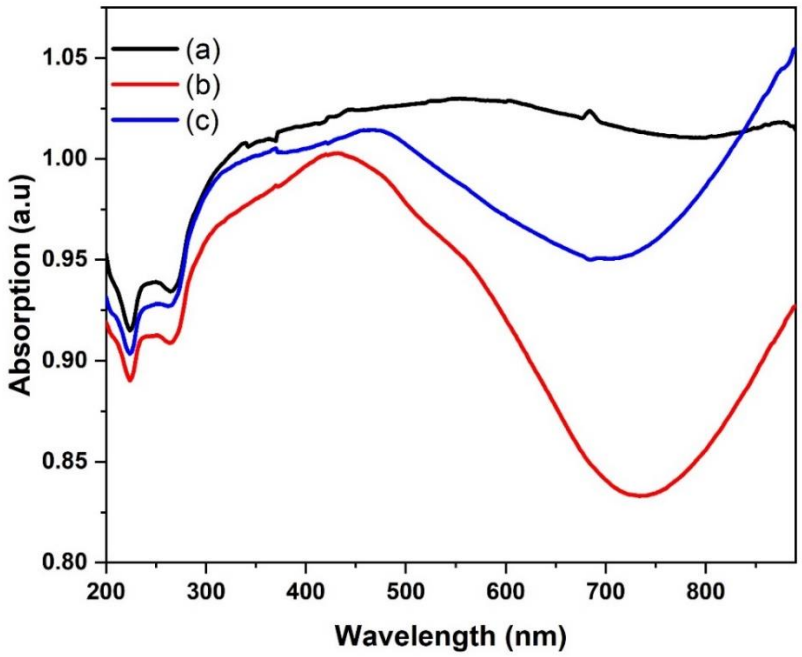

Figure 5: UV-Vis absorption spectra of Fe_3O_4 NPs a) 200 ^oC, b) 250 ^oC, c) 300 ^oC.

4. Conclusions

In summary, Fe_3O_4 NPs formed via the solvothermal route were thoroughly characterized for their crystallinity, surface morphology, particle size distribution, and optical properties. Powder XRD analysis showed that the as-synthesized Fe_3O_4 NPs had an inverse spline structure and were crystalline in nature. SEM analysis indicated that the spherical morphology of the particles was aggregated. The elemental composition of the Fe_3O_4 NPs was confirmed using EDX analysis. Furthermore, the optical properties of Fe_3O_4 NPs are indicated in the visible region in the wavelength range of 420–580 nm. In addition, we observed a red shift at 200 °C and a blue shift at 250 and 300 °C. Such shifts can be attributed to the availability of oxygen vacancies and quantum size effects in the nanocrystals produced during solvothermal synthesis.

Conflicts of interest

The authors declare no conflict of interest.

Acknowledgements

The author RV and JM are thankful to Ms. S.K. Vivetha M.Sc. student for her support during the experiment, JM thank RUSA, UPE, FIST, and DST – PURSE programme MK University, for providing the XRD, SEM, and UV facilities.

References

1. D. Mangalam, D. Manoharadoss, P. Karuppasamy, S. Manickam Mahendran. Structural, Optical, Morphological and Dielectric Properties of Cerium Oxide Nanoparticles. *Mat. Res*. 2016: 19; 478-482.

2. P. Raj, K. Sadaiyandi, K. Kennedy, A. et al. Influence of Mg Doping on ZnO Nanoparticles for Enhanced Photocatalytic Evaluation and Antibacterial Analysis. *Nanoscale Res Lett*. 2018: 13; 229.

3. Y. Yew, P. Shameli, K. Miyake, M. Kuwano, N. Khairudin, N. B. B. A. Mohamad, S. E. B., & Lee, K. X. Green synthesis of magnetite (Fe_3O_4) nanoparticles using seaweed. *Nanoscale research letters* .2016: 11; 1-7.

4. Malakootian, M. Askarpuor, A. Amirmahani, N. Nasiri, Z. Nasiri, A. Removal of Hexavalent Chromium from Aqueous Solutions Using Magnetic Nanoparticles Coated with Alumina and Modified by Cetyl Trimethyl Ammonium Bromide. *Journals of Community Health Research*. 2015: 4; 177-193.

5. M. Cavas, R.K. Gupta, Ahmed A. Al-Ghamdi, Zarah H. Gafer, Farid El-Tantawy, F. Yakuphanoglu, Preparation and characterization of dye sensitized solar cell based on nanostructured Fe_2O_3. *Mater. Lett*. 2013: 105;106-109.

6. R.K. Gupta, K. Ghosh, R. Patel, P.K. Kahol, A novel method to synthesis iron oxide thin films. *J. Alloys Compd*. 2011: 509; 7529-7531.

7. R.K. Gupta, K. Ghosh, L. Dong, P.K. Kahol. Structural and magnetic properties of phase-controlled iron oxide rods. *Mater. Lett*. 2011: 65; 225-228.

8. S. Sun and H. Zeng. Size-Controlled Synthesis of Magnetite Nanoparticles. *J. Am. Chem. Soc*. 2002: 124; 8204 -8205.

9. S. Peng and S. Sun, Angew. Synthesis and characterization of monodisperse hollow Fe_3O_4 nanoparticles. *Angew Chem., Int. Ed. 46.* 2007: 22; 4155-8.

10. B. Tian, X. Yu, Li and K. Li. Facile solvothermal synthesis of monodisperse Fe_3O_4 nanocrystals with precise size control of one nanometre as potential MRI contrast agents, *J. Mater. Chem*. 2011: 21; 2476.

11. P. L. Taberna, S. Mitra, P. Poizot, P. Simon, and J. M. Tarascon, High rate capabilities Fe_3O4-based Cu nano-architectured electrodes for lithium-ion battery applications. *NatureMater*. 2006: 5 ;7; 567-73.

12. M. R. McCartney and D. J. Smith, Electron Holography: Phase Imaging with Nanometer Resolution. *Annu. Rev. Mater. Res*. 2007: 37; 729.

13. X.D. Liu, H. Chen, S.S. Liu, L.Q. Ye, Y.P. Li, Hydrothermal synthesis of superpara-magnetic Fe_3O_4 nanoparticles with ionic liquids as stabilizer. *Mater. Res. Bull*. 2015: 62 ; 217–221.

14. F.X. Chen, S.L. Xie, J.H. Zhang, R. Liu, Synthesis of spherical Fe_3O_4 magnetic nanoparticles by co-precipitation in choline chloride/urea deep eutectic sol-vent. *Mater. Lett*.2013: 112 ; 177–179.

15. H.T. Cui, Y. Liu, W.Z. Ren, Structure switch between α-Fe_2O_3, γ-$Fe_2O_3$and Fe_3O_4 during the large scale and low temperature sol–gel synthesis of nearly monodispersed iron oxide nanoparticles, *Adv. Powder Technol*. 2013: 24; 93–97.

16. K. Chinnaraj, A. Manikandan, P. Ramu, S. Arul Antony, P. Neeraja, Compara-tive studies of microwave-and sol–gel-assisted combustion methods of Fe_3O_4 nanostructures: structural, morphological, optical, magnetic, and catalytic prop-erties. *J. Supercond. Nov. Magn*. 2015: 28; 179–190.

17. Y.F. Li, R.L. Jiang, T.Y. Liu, H. Lv, L. Zhou, X.Y. Zhang, One-pot synthesis of grass-like Fe_3O_4 nanostructures by a novel microemulsion-assisted solvother-mal method. *Ceram. Int*. 2014: 40 ; 1059–1063.

18. Z. Fekri Leila, N. Mohammad, H. Pour Keyhan, Green aqueous synthesis of mono, bis and trisdihydropyridines using nano Fe3O4under ultrasound irra-diation. *Curr. Org. Synth*. 2015: 12 ; 76–79.

19. J.H. Yang, B. Ramaraj Kuk Ro Yoon, Preparation and characterization of super-paramagnetic graphene oxide nanohybrids anchored with Fe3O4nanoparticles. *J. Alloys Compd*. 2014: 583; 128–133.

20. Z.P. Cheng, X.Z. Chu, J.Z. Yin, H. Zhong, J.M. Xu, Surfactantless synthesis of Fe_3O_4 magnetic nanobelts by a simple hydrothermal process. *Mater. Lett*. 2012: 75; 172–174.

21. Y. Takeno, Yasukazu Murakami, Takeshi Sato, Toshiaki Tanigaki, Hyun Soon Park, Daisuke Shindo, R. Matthew Ferguson, Kannan M. Krishnan, Morphology and magnetic flux distribution in superparamagnetic, single-crystalline Fe3O4 nanoparticle rings. *Appl. Phys. Lett*. 2014: 105 ; 183102.

22. S.J. Yan, J.K. Tang, P. Liu, Q. Gao, G.Y. Hong, L. Zhen, The influence of hollow structure on the magnetic characteristics for Fe3O4 submicron spheres. *J. Appl. Phys.* 2011: 109 ; 07B535.

23. K. He, F. Xiang Ma, C. Yan Xu, and J. Cumings, Mapping magnetic fields of Fe_3O_4 nanosphere assemblies by electron holography. *Journal of Applied Physics*. 2013: 113; 17B528

24. Wu, W., He, Q. & Jiang, C. Magnetic Iron Oxide Nanoparticles: Synthesis and Surface Functionalization Strategies. *Nanoscale Res Lett*. 2008: 3; 397.

25. S.Vikram, R. Vasanthakumari, T. Suzuki. Investigations of suspension stability of iron oxide nanoparticles using time-resolved UV–visible spectroscopy. *J Nanopart Res*. 2016: 18; 272